Research Square

Preprints are preliminary reports that have not undergone peer review.
They should not be considered conclusive, used to inform clinical practice,
or referenced by the media as validated information.

Heterogeneous structural deficits across lower-leg agonist– antagonist muscle groups in children with cerebral palsy: a cross-sectional imaging study

Zhenhao Liu
University of North Carolina at Chapel Hill
Geoffrey Handsfield
geoffrey_handsfield@med.unc.edu
University of North Carolina at Chapel Hill

Research Article

Keywords: diffusion tensor imaging, musculoskeletal biomechanics, computational modeling, fiber tractography, MRI, DTI

Posted Date: October 30th, 2026

DOI: https://doi.org/10.21203/rs.3.rs-11236586/v1

License: This work is licensed under a Creative Commons Attribution 4.0 International License.
Read Full License

Additional Declarations: No competing interests reported.

Heterogeneous structural deficits across lower-leg agonist–antagonist muscle groups in children with cerebral palsy: a cross-sectional imaging study

Zhenhao Liu[1,2], *Geoffrey Handsfield[1,2]

[1]Department of Orthopaedics, University of North Carolina at Chapel Hill, Chapel Hill, NC, USA

[2]Lampe Joint Department of Biomedical Engineering, University of North Carolina at Chapel Hill and NC State University, Chapel Hill, NC, USA

*Corresponding author's email: geoffrey_handsfield@med.unc.edu

Abstract

Structural alterations in skeletal muscle in cerebral palsy (CP) directly contribute to joint stiffness and impaired motor control, and govern the outcome of rehabilitative interventions. Diffusion tensor imaging (DTI) has established architectural alterations in individual lower-limb muscles, but previous work has focused on a small subset of plantarflexor muscles in isolation, leaving their antagonists uncharacterized despite the reciprocal relationships between muscle pairs crossing the same joint. Because imbalance between such pairs is linked to gait limitations, characterizing whether architectural deficits in CP are proportional across agonist-antagonist pairs, or instead reflect atypical antagonist co-activation, is important. In this study, MRI and DTI data from nine children with CP (10.6 ± 2.2 years, GMFCS I–III) and nine age- and sex-matched typically developing controls from a previous study were used to assess muscle size and architecture in

seven muscles and muscle groups in the leg. Volume and muscle length were determined from segmented surface meshes; physiological cross-sectional surfaces (PCSS), fascicle length, and angle were computed from DTI tractography; fractional anisotropy and mean diffusivity were determined from diffusion tensor data. Normalized muscle volume of examined muscles was 38.8% lower in CP ($g = -2.71$) and PCSS 27.2% lower ($g = -2.18$, both $p < 0.001$). Volume (−29.2% to −41.3%) and muscle length (−9.5% to −12.2%, all $p_fdr \leq 0.004$) were reduced in all four functional muscle groups of the leg, but the composition of that loss differed: dorsiflexor volume fell almost entirely through cross-sectional thinning (PCSS −26.6%, fascicle length −0.9%), the invertor almost entirely through fascicle shortening (−3.4%, −26.1%), and the plantarflexors through both (−28.6%, −31.5%). Plantarflexor:dorsiflexor and invertor:evertor size ratios did not differ, though the sample supports only effects of $g \geq 1.41$. Individually, 33% of CP participants exceeded $|z| > 2$ on invertor:evertor ratio, driven by an undersized evertor, and volume z-scores exceeded $|z| > 2$ in 41% of muscle-participant combinations. Fascicle orientation was more uniformly aligned in tibialis anterior, and more dispersed in posterior soleus. Muscle deficits in CP were pervasive but heterogeneous, with clinically relevant imbalance emerging at the individual level despite proportional group averages.

Keywords: diffusion tensor imaging; musculoskeletal biomechanics; computational modeling; fiber tractography; MRI; DTI

Introduction

Cerebral palsy (CP) is the most common cause of childhood physical disability and is frequently accompanied by progressive musculoskeletal complications that extend beyond the primary neural injury (1–3). Individuals with CP often develop joint contractures, reduced muscle size, and

reduced mobility, particularly in the lower limbs. These secondary impairments reflect long-term adaptations in both neuromuscular control and muscle structure that develop with growth and repeated movement patterns (2,3). Because muscle is the effector that converts neural commands into joint motion, its structural state shapes the outcome of rehabilitation approaches such as physical therapies, functional electrical stimulation, and orthoses (4). Quantitative, muscle-specific measures are therefore needed to guide and personalize these interventions (5).

One characteristic of CP is elevated agonist-antagonist co-activation relative to typically developing (TD) individuals, commonly quantified via a co-contraction index (6). At the ankle, this mechanism has been best characterized for the plantarflexor-dorsiflexor pair, which acts in the sagittal plane (6): the plantarflexor functions as the agonist during the toe-off phase of gait, while the dorsiflexor acts as its antagonist. In CP, excessive or poorly timed activation of the antagonist during agonist-driven movement can reduce joint range of motion and modify mechanical loading on muscle (7,8). Over time, these altered loading conditions may contribute to adaptive remodeling of muscle architecture, reinforcing limitations in the muscle's ability to generate force (9). Prior studies in CP have reported architectural alterations including shorter fascicles, altered pennation angle, reduced muscle volume, and increased stiffness in specific muscles (10–12).

The invertors and evertors deserve separate consideration. These muscles control foot position and subtalar stability during stance and swing, and imbalance between them is implicated in varus and valgus foot deformities that impair gait and frequently lead to orthotic or surgical management, such as tendon transfers (13). Although this pair is not usually framed in terms of co-activation, its

function depends on the balance between opposing muscles, and whether that balance is structurally altered in CP is largely unknown (14).

Most existing *in vivo* muscle architectural assessments rely on ultrasound or diffusion tensor imaging (DTI) (15). Ultrasound can estimate fascicle length and pennation angle, but measurements are limited to a two-dimensional plane and may not capture regional heterogeneity across the whole muscle. DTI provides a noninvasive method to infer three-dimensional (3D) muscle fiber orientation by measuring directionality of water diffusion within tissue (16,17). Using DTI, fiber tractography can be reconstructed to represent 3D muscle architecture and diffusion tensors can be extracted to reflect tissue organization and muscle quality (11,17,18).

Although DTI has been applied to musculoskeletal questions in CP, most studies have focused on a limited subset of plantarflexor muscles (11,12,19,20), while the architecture of its antagonist muscles remains poorly characterized. Understanding the agonist–antagonist muscle pairs around the ankle is particularly important, because they contributes to ankle joint stiffness and stability, and altered co-activation at the ankle is associated with reduced joint excursion during gait (6,8) and with impaired reactive balance control in CP (21).

This study uses DTI to assess ankle agonist–antagonist muscle size and architecture in individuals with CP compared to TD controls. We characterize 3D muscle architecture across four functional ankle muscle groups: plantarflexors, dorsiflexors, invertors, and evertors, and distinguish generalized muscle loss from deficits confined to particular regions of the limb. We hypothesize that (i) muscle size is reduced and fascicle architecture altered in CP across all four functional

groups; (ii) the ratios of muscle morphology between each agonist–antagonist pair differ from TD, indicating an altered balance between opposing muscle groups; and (iii) deficits are not uniform across the limb, with some regions disproportionately affected relative to the rest of the limb. By profiling muscle architecture, this work aims to provide measures that can inform targeted surgical and rehabilitative decisions in CP.

Method

Participants

A total of 18 volunteers were included in this study, comprising nine individuals with CP and nine TD controls. De-identified muscle image data were used from a previously published study (12). That study's protocol was approved by the University of Auckland Human Participants Ethics Committee. Written informed consent was obtained from the participants' parents or legal guardians before participation, and all children provided assent to take part in the study. The CP group consisted of volunteers (8-13 years, 5 males/4 females) with a clinical diagnosis of cerebral palsy confirmed by an experienced clinician. Participants showed hemiplegic (n=4) or diplegic (n=5) involvement affecting the lower limbs; spasticity was observed in six of the nine participants. Functional severity ranged from GMFCS levels I-III (I: n=2; II: n=5; III: n=2). All children could follow simple verbal instructions and tolerate MRI. None had undergone orthopedic or neurosurgical interventions within the previous 12 months, and none had additional neurological/genetic disorders, severe fixed contractures, or MRI contraindications. The TD control group comprised age- and gender-matched volunteers (7-14 years, 5 males/4 females) with no history of neurological, neuromuscular, or musculoskeletal disorders, all of whom could complete MRI procedures. All participant characteristics are provided in Table 1.

Table1. Characteristics of all subjects.

Group	Sex (F/M)	Age (years)	Height (m)	Weight (kg)	Spasticity (Yes/No)	Hemi/ Diplegic	GMFCS (I/II/III)
CP (n=9)	4/5	10.6 ± 2.2	1.4 ± 0.1	33.8 ± 11.8	6/3	4/5	2/5/2
TD (n=9)	4/5	10.9 ± 2.4	1.5 ± 0.1	36.4 ± 9.6	/	/	/

MRI acquisition

Full details of the MRI acquisition can be found in the original study (12). Briefly, participants were scanned feet-first supine with the target leg centered in the magnet. A single limb was imaged for each participant. In the CP group, the more affected limb was scanned, while in TD a limb was selected at random. Foam pads minimized leg motion and to maintain a neutral ankle angle. Images were acquired on a 3-Tesla MRI scanner (Skyra, Siemens Healthineers, Erlangen, Germany) using the body coil for transmission. A 3D T1-weighted VIBE sequence was used, oriented to the sagittal plane. Imaging parameters were TR/TE: 10.4/5.22 ms, flip angle: 10°, field of view: 128 × 228 × 384 (mm×mm×mm), with isotropic spatial resolution of 0.8 mm. DTI used a 2D echo-planar diffusion-weighted sequence with fat suppression (Fig. 1B). Sequence parameters were TR/TE: 4400/74 ms, flip angle: 90°, field of view: 200 × 200 × 5 (mm×mm×mm), spatial resolution: 1.64 × 1.64 (mm×mm), with 5mm slice thickness. Two stacks of DTI were collected with 35 transverse slices for each stack. Twenty diffusion-encoding directions were acquired at a b-value of 500 s/mm² with one signal average.

Imaging processing

Image data were resampled to 5 mm slice thickness using a custom python script. The two DTI stacks were stitched to reconstruct the full scan volume. Target muscles were classified by their main function on the ankle joint (Fig. 1A). Tibialis anterior (TA) and the extensor group (EXT: extensor digitorum longus, extensor hallucis longus, and peroneus tertius) were classified as dorsiflexors, whereas medial gastrocnemius (MG), lateral gastrocnemius (LG), and soleus (SOL) were classified as plantarflexors, forming an agonist-antagonist pair. SOL was divided into 4 subregions according to the architecture, including anteromedial (SOL-AM), anterolateral (SOL-AL), posteromedial (SOL-PM), and posterolateral (SOL-PL) (22). For inversion-eversion, tibialis posterior (TP) was designated as the primary inverter and the peroneals (PER: peroneus longus and brevis) were grouped as evertors. Target muscles were semi-automatically segmented on the resampled T1-VIBE images and the Tracew images using nn-Interactive in ITK-SNAP 4.4.0, which served as anatomical reference and DTI mapping, respectively (23,24). All resulting masks were subsequently reviewed and manually refined.

DTI data were processed using MRtrix3 (version 3.0.8) (25), including denoising, Gibbs-ringing correction, motion and eddy-current correction, and bias-field correction. Diffusion tensors were then fitted to derive fractional anisotropy (FA) and mean diffusivity (MD) maps. For tractography, muscle masks were eroded to generate separate seed and tracking masks, with tracking further restricted to voxels falling within an MD-based inclusion range. Streamline tracking was performed using a deterministic tensor-based algorithm, with seeds placed in the muscle interior and tracking constrained to the muscle tracking mask (Fig. 1D & Fig. 2). Tracking used a step size of 0.5 mm, a maximum turning angle of 30°, length limits of 10–200 mm, and an FA stopping threshold of 0.05–0.35 (determined adaptively per muscle from its local FA distribution),

continuing until 3,000 streamlines were generated per muscle. For the soleus in the CP group, a wider length range (5–200 mm) and larger turning angle (45°) were used to account for its complex architecture and distortion, which otherwise resulted in premature streamline termination under the default parameters; the resulting streamlines were subject to the same filtering criteria described below.

Muscle morphology and architecture

Muscle length was defined as the arc length of the centroid line (Fig. 1C), which is the primary mesh axis estimated by principal component analysis. Muscle volume was calculated from the closed surface mesh. The muscle volume was scaled by body weight and height, and length was normalized by height (12).

Muscle fiber tractography streamlines (Fig. 2) were first filtered by length, tortuosity, maximum turning angle, and local directional coherence with neighboring fibers, retaining only coherent, fascicle-like streamlines. Each streamline endpoint was then extended or clipped to the muscle surface mesh via curvature-following ray–mesh intersection, depending on whether the endpoint fell inside or outside the muscle volume. Fascicle length was computed as the arc length of the endpoint-extended streamline and then normalized by height (Fig. 1E). The line of action was defined as the first principal component of all fascicle points pooled within a muscle, giving a straight axis through the fascicle field. Fascicle angle was computed as the acute angle between the local tangent of the fascicle and the local tangent of the line of action at the nearest correspondence point and reported in degrees (Fig. 1E). For each streamline, fascicle angle was summarized as the mean across all pointwise correspondences. To characterize the shape of each

muscle's fascicle-angle distribution, per-fascicle angles were pooled within each participant's muscle and reduced to ten subject-level descriptors: the minimum, 10th, 25th, 50th, 75th and 90th percentiles, maximum, mean, standard deviation (SD), and interquartile range (IQR).

Tract tortuosity was quantified using a length-based index, defined as the ratio of the tract's arc length to the straight-line (Euclidean) distance between its two endpoints (Fig. 1F). A tortuosity value of 1 indicates a perfectly straight tract, with larger values indicating greater path curviness. Tortuosity was computed for each endpoint-extended streamline and summarized as the mean across all tracts.

Physiological cross-sectional surface

The physiological cross-sectional surface (PCSS) is a representation of all the muscle fibers acting in parallel in complex 3D muscle geometries (26). PCSS comprises a finite number of curved surfaces fitted inside the muscle volume where each surface is everywhere perpendicular to the local fiber direction and intersects every fiber. The PCSS is a substitute for physiological cross sectional area in complex 3D muscle shapes, where the curved surfaces replace the single flat cutting plane assumed by conventional physiological cross sectional area (26,27). PCSS was estimated from reconstructed fiber trajectories: local fiber direction was interpolated via k-nearest-neighbor weighting of tangent vectors, and a scalar potential field was fit on a grid within the muscle volume so that its gradient aligned with this direction. PCSS sub-surfaces were generated in cases where the main surface did not capture all fibers in parallel (Fig. 1G).

Diffusion tensor metrics

Diffusion tensor metrics were computed in Python using DIPY. For each muscle, the mask was applied to restrict the analysis to voxels within the muscle region. A diffusion tensor model was then fit using the masked diffusion-weighted data together with the corresponding b-values and b-vectors. From the fitted tensor, voxel-wise scalar indices were derived, including FA and MD.

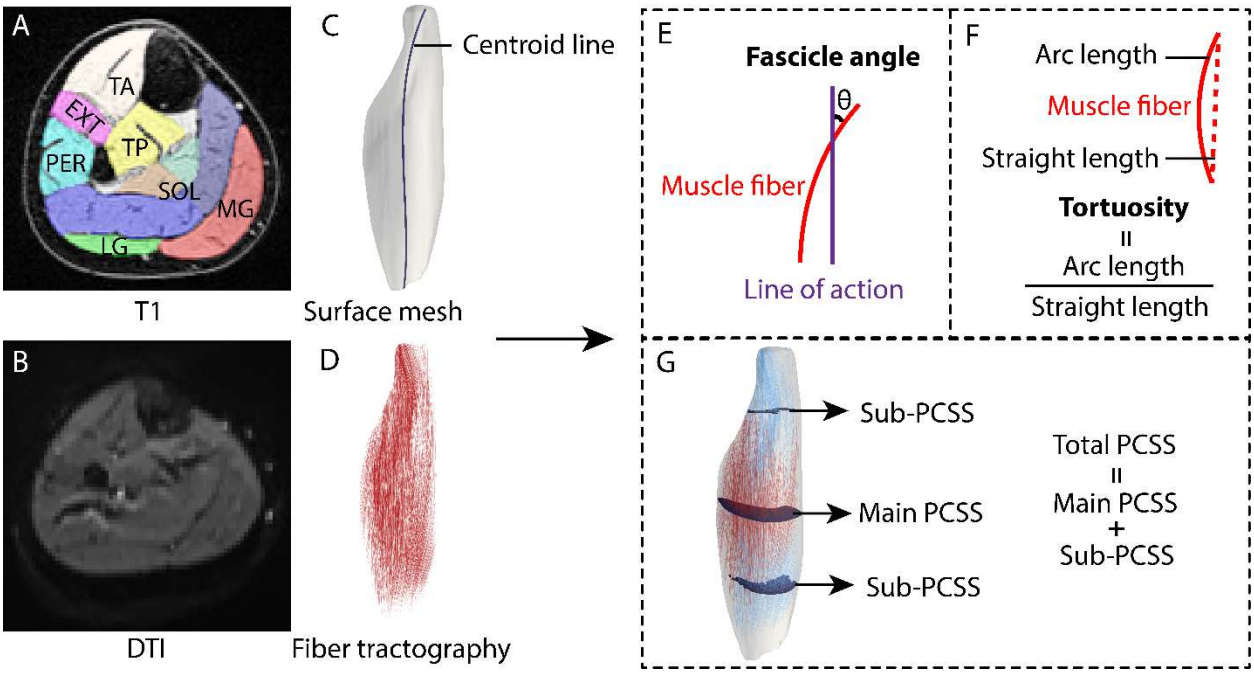


Figure 1. Imaging, model reconstruction, and architectural measures. (A) Representative axial T1-weighted VIBE image of the lower leg with the segmented regions overlaid: tibialis anterior (TA), extensor group (EXT), peroneals (PER), tibialis posterior (TP), medial gastrocnemius (MG) and lateral gastrocnemius (LG), and soleus (SOL), shown as its four compartments (SOL-AM, SOL-AL, SOL-PM, SOL-PL). (B) Corresponding axial diffusion tensor image (DTI). (C) Surface mesh reconstructed from the segmentation; muscle length was defined as the arc length of the centroid line (blue). (D) Fiber tractography reconstructed from the DTI shown for MG. (E) Fascicle angle θ between the local tangent of the fascicle (red) and the local tangent of the muscle line of action (purple). (F) Fascicle tortuosity, the ratio of fascicle arc length to the straight-line distance between its endpoints. (G) Physiological cross-sectional surface (PCSS): curved surfaces

fitted within the muscle volume that remain locally perpendicular to the local fiber direction and intersects all fibers.

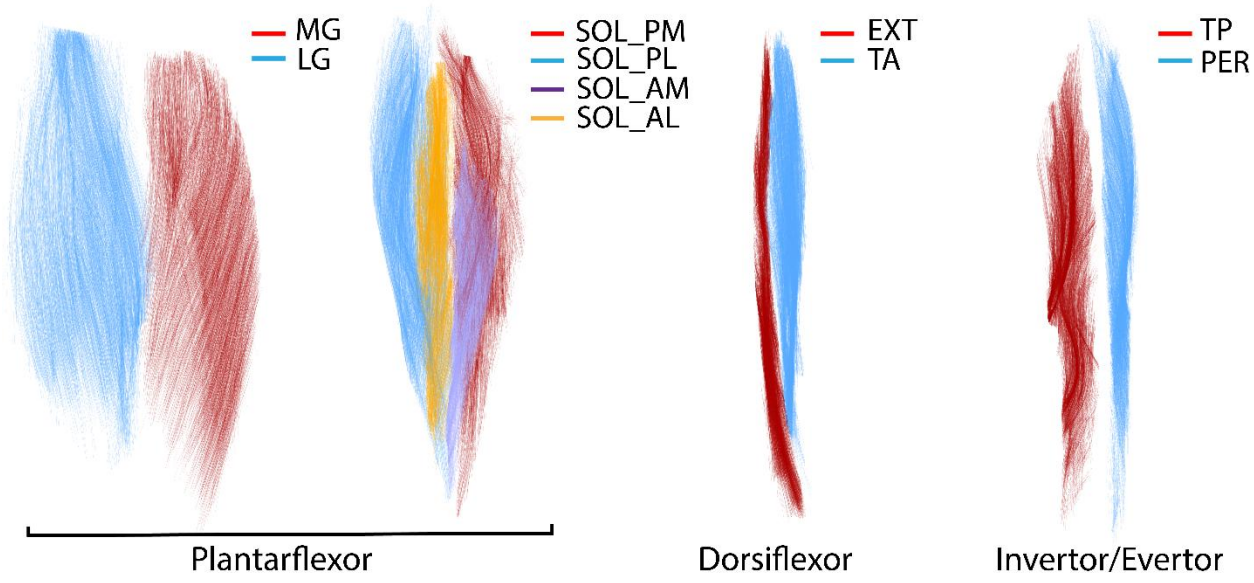


Figure 2. Representative fiber tractography of the ankle functional muscle groups. Reconstructed fascicles of target muscles from a CP and a TD participant, viewed with proximal at the top. Abbreviations as in Figure 1.

Statistical analysis

With nine participants per group, all comparisons used exact permutation tests, recomputing the statistic for all 48,620 possible splits of the 18 participants into two groups of nine. This gives an exact p-value without distributional assumptions. Effect sizes are Hedges' g with bootstrap 95% confidence intervals.

Agonist–antagonist balance was assessed from within-participant ratios of one muscle group to its antagonist. To identify regions affected more than the limb as a whole, each region was expressed as a fraction of that participant's mean across the ten regions, and the CP–TD difference in this

fraction was compared between groups: a negative difference indicates a disproportionate deficit, a positive difference relative sparing.

Benjamini–Hochberg false discovery rate (FDR) was applied within each metric. The agonist–antagonist ratio comparisons and the within-limb regional comparisons were verified by leave-one-out resampling, in which each participant was removed in turn and the analysis repeated; the largest resulting unadjusted p-value is reported as the worst case. Data were screened before analysis for physically implausible values and for systematic subject-level deviation indicating scan artefact, using technical criteria only and blind to the group comparison; no participant was excluded. With nine participants per group, an effect of $g = 1.41$ was detectable with 80% power at $\alpha = 0.05$; smaller effects remained detectable with correspondingly lower power. Non-significant results therefore indicate that a difference could not be detected rather than that none exists.

Fascicle-angle distribution descriptors were compared with the same exact permutation test, with FDR correction applied across the ten muscles within each descriptor. A z-score was computed for each CP participant on every muscle × metric combination as (participant value − TD mean) / TD SD, and combinations with $|z| > 2$ were flagged as deviating from the TD reference. All analyses used Python 3.12.

Results

Throughout, p denotes unadjusted exact permutation p-values and p_fdr denotes FDR adjusted values. All comparisons are CP relative to TD. Values in text are reported as mean ± SD where

given; elsewhere as percent difference and Hedges' g; figures show group means ± standard error of the mean (SEM).

Muscle size and architecture

Total normalized volume across the examined ankle muscles was 38.8% lower in CP (11.17 ± 2.69 vs 18.24 ± 2.27 $cm^3 \cdot kg^{-1} \cdot m^{-1}$, $g = -2.71$, $p < 0.001$) and total normalized PCSS 27.2% lower (1.53 ± 0.30 vs 2.10 ± 0.19 $cm^2 \cdot kg^{-1}$, $g = -2.18$, $p < 0.001$). Normalized volume was lower in all four functional groups (−29.2% to −41.3%, all $p_fdr \leq 0.004$) and normalized PCSS was lower in plantarflexors (−28.6%, $p_fdr < 0.001$), dorsiflexors (−26.6%, $p_fdr = 0.020$), and evertors (−36.0%, $p_fdr = 0.020$), but not invertors (−3.4%, $p_fdr = 0.86$). Normalized muscle length was lower in all four groups (−9.5% to −12.2%, $p_fdr \leq 0.004$) (Fig. 3).

Normalized plantarflexor fascicle length were 31.5% shorter ($g = -2.45$, $p_fdr = 0.001$) and invertor fascicle length were 26.1% shorter ($g = -1.32$, $p_fdr = 0.016$), whereas dorsiflexor and evertor fascicle length did not differ (−0.9%, $p_fdr = 0.89$; −16.1%, $p_fdr = 0.14$). Fascicle angle did not differ in any functional group ($p_fdr \geq 0.053$), nor did FA ($p_fdr \geq 0.097$) or MD ($p_fdr \geq 0.102$). Tract tortuosity was lower in evertors (1.006 vs 1.017, $p_fdr = 0.049$) and did not differ elsewhere. At the individual-muscle level, however, mean fascicle angle was lower in TA (−30.3%, $g = -1.52$, $p_fdr = 0.032$) and higher in SOL-PM (+46.8%, $g = 1.42$, $p_fdr = 0.032$); MD was lower in TA (−7.4%, $g = -1.62$, $p_fdr = 0.026$); and FA was lower in SOL-AL (−20.8%, $g = -1.28$, $p_fdr = 0.043$) and SOL-PL (−17.5%, $g = -1.31$, $p_fdr = 0.043$) (Fig. 4). Across all metrics, 31 of 80 individual-region comparisons reached $p_fdr < 0.05$, most frequently for volume (9 of 10 regions) and muscle length (7 of 10 regions).

Pooling all individual fascicles within each muscle showed that the shape of the orientation distribution changed in TA and SOL-PM, and in opposite directions (Fig. 5). In TA, the upper tail of the distribution was compressed in CP: the 75th and 90th percentiles were 30.1% and 31.0% lower than TD (9.1° vs 13.0°, g = −1.47, p_fdr = 0.032; 11.4° vs 16.5°, g = −1.71, p_fdr = 0.011). The opposite pattern occurred in SOL-PM, where the distribution was more dispersed in CP: the SD was 81.8% higher (16.2° vs 8.9°, g = 1.83, p_fdr = 0.009), and the 75th and 90th percentiles were 56.8% and 68.8% higher (47.5° vs 30.3°, g = 1.55, p_fdr = 0.032; 59.1° vs 35.0°, g = 1.88, p_fdr = 0.011). No other muscle reached significance on any descriptor, and no other descriptor reached significance in any muscle. The strongest non-significant result was the 75th percentile in SOL-PL (54.2% higher, g = 1.20, p_fdr = 0.052).

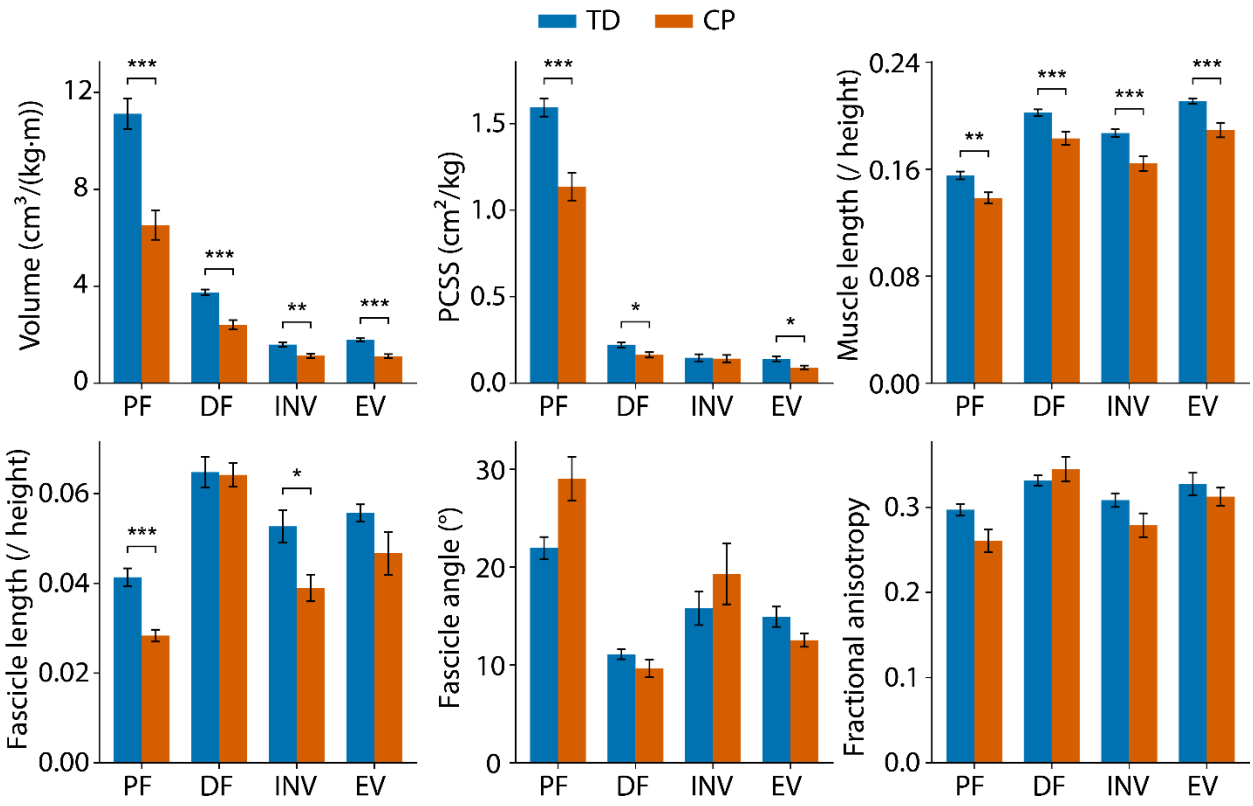


Figure 3. Muscle size and architecture by ankle functional group. Group means ± SEM (TD, blue; CP, orange). PF, plantarflexors; DF, dorsiflexors; INV, invertor; EV, evertors. Brackets mark differences surviving FDR correction across functional groups within each metric: *q < 0.05, **q < 0.01, ***q < 0.001.

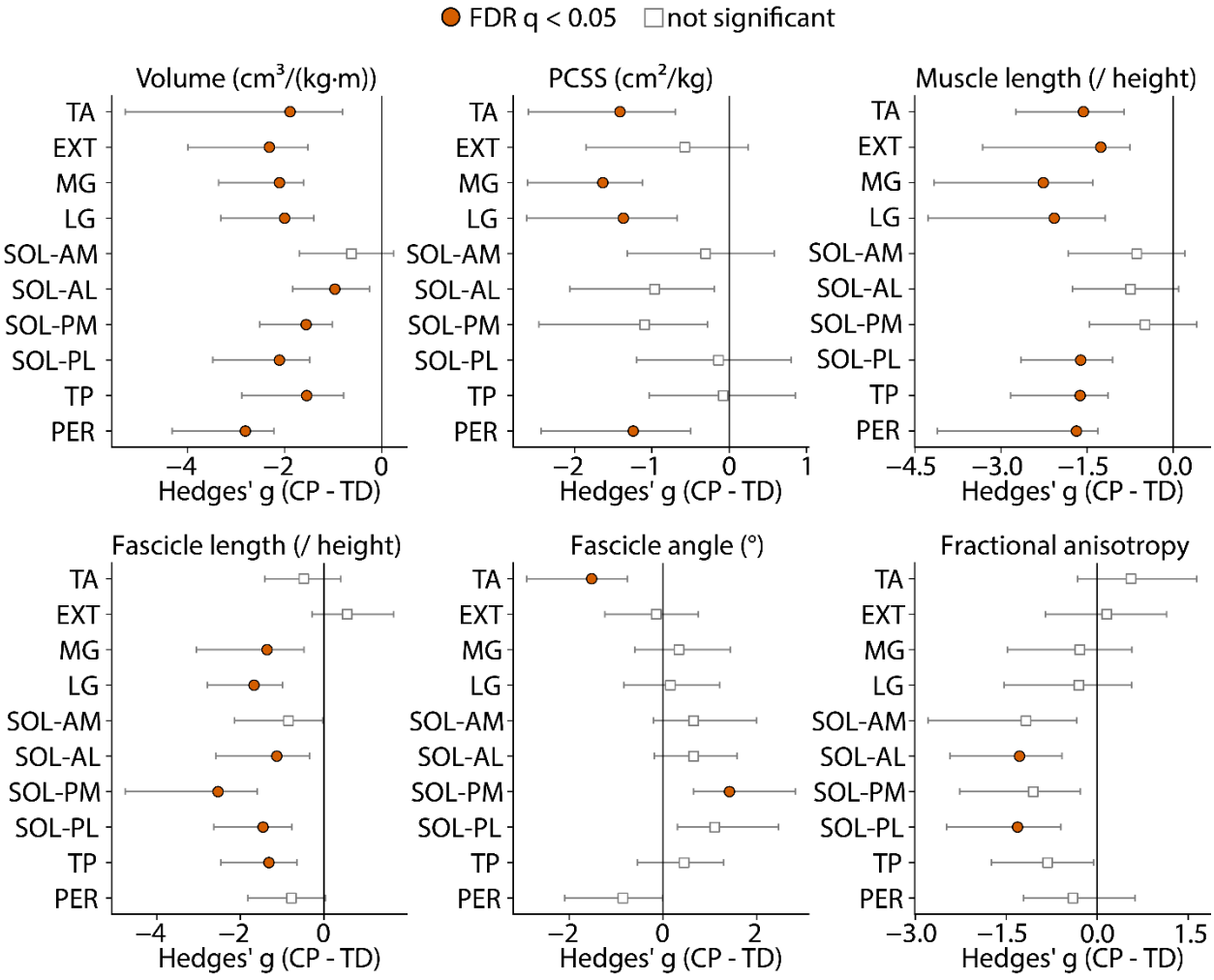


Figure 4. Per-muscle effect sizes, CP versus TD. Hedges' g with bootstrap 95% confidence intervals; negative values indicate lower values in CP. Filled orange circles, FDR q < 0.05; open grey squares, not significant. Size and length measures are normalized to body size; fascicle angle and fractional anisotropy are analyzed as measured. Abbreviations as in Figure 1.

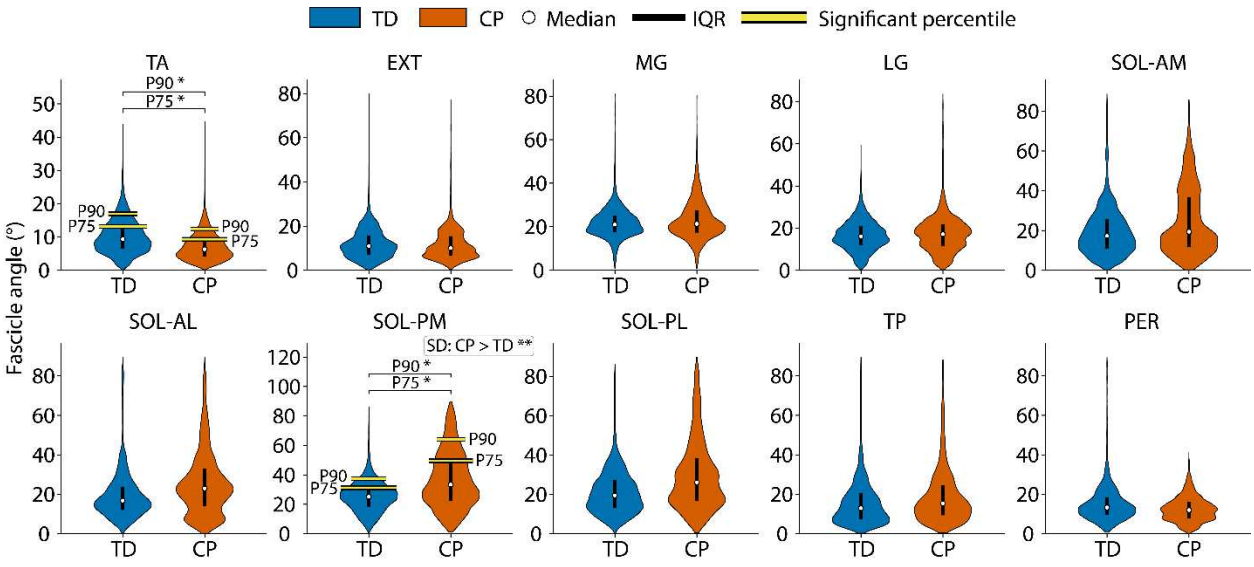


Figure 5. Distribution of individual fascicle angles within each region. Violin plots pool every retained fascicle from all participants in a group (TD, blue; CP, orange). White dot, group median; black bar, interquartile range. Yellow lines mark a percentile descriptor that differed significantly between groups after FDR correction. The bracket above the violins gives its significance level. Boxed notes give significant spread descriptors and the direction of the difference. *q < 0.05, **q < 0.01, ***q < 0.001. Abbreviations as in Figure 1.

Agonist–antagonist balance

No imbalance was detected in CP. The plantarflexor:dorsiflexor ratio was 2.72 ± 0.53 in CP versus 2.99 ± 0.54 in TD for volume (g = −0.48, p = 0.29, p_fdr = 0.39) and 7.36 ± 2.09 versus 7.46 ± 1.82 for PCSS (g = −0.05, p = 0.91, p_fdr = 0.91). The invertor:evertor ratio was 1.05 ± 0.33 versus 0.89 ± 0.10 for volume (g = 0.64, p = 0.17, p_fdr = 0.35) and 2.09 ± 1.72 versus 1.08 ± 0.42 for PCSS (g = 0.77, p = 0.12, p_fdr = 0.35) (Fig. 6).

At the individual level, however, the invertor:evertor ratio contained a subset of clear outliers: 3 of 9 CP participants exceeded $|z| > 2$ against the TD reference distribution for volume, and 3 of 9 for PCSS, versus 0 of 9 for plantarflexor:dorsiflexor on either metric (Fig. 6). In every flagged case the deviation was driven by a disproportionately small evertor, not an enlarged invertor, consistent with the reduced evertor PCSS reported above.

Despite the preserved group-level balance, individual CP participants deviated from the TD reference distribution in absolute size. Muscle-volume z-scores exceeded $|z| > 2$ in 41.1% of subject × muscle combinations, and PCSS z-scores in 10.0% (Fig. 7).

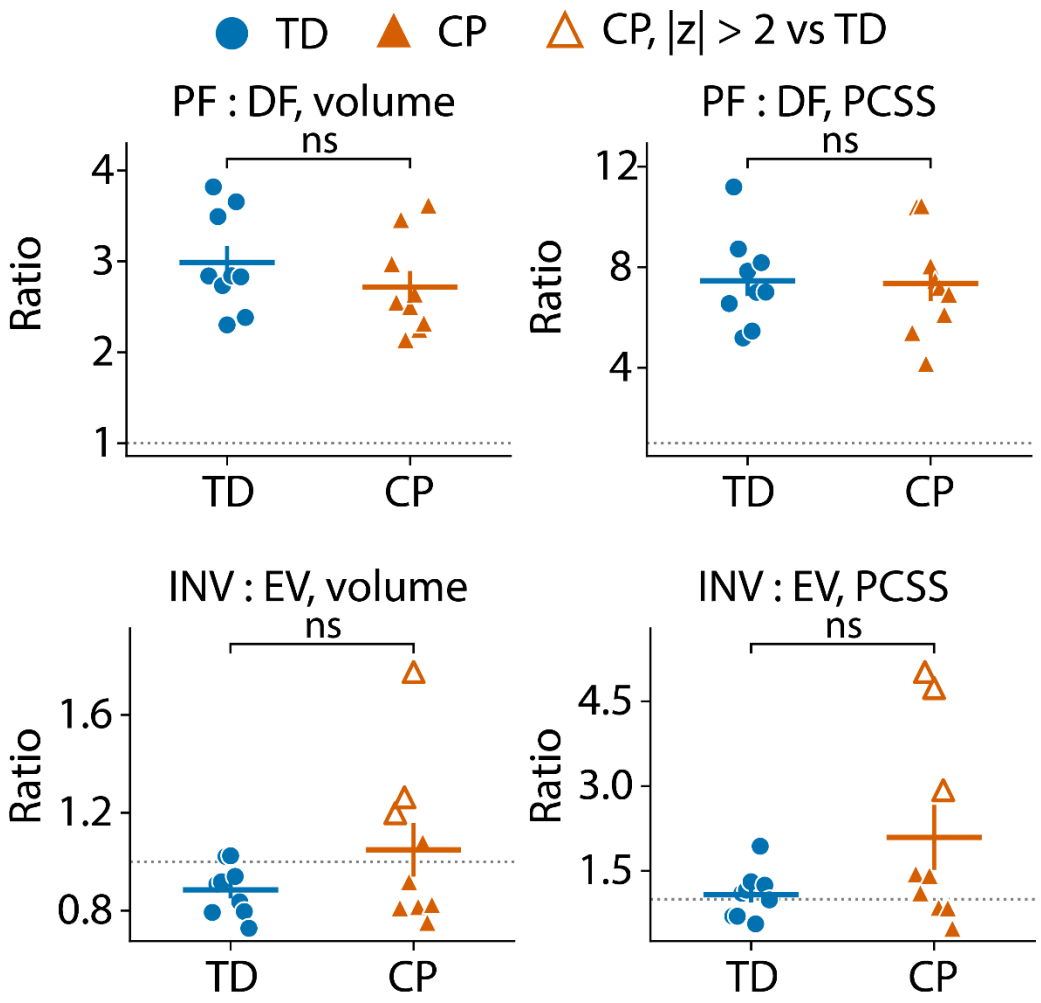


Figure 6. Agonist–antagonist size ratios. Individual participants (TD, blue circles; CP, orange triangles) with group mean ± SEM. Hollow orange triangle, CP participant with $|z| > 2$ versus the TD reference distribution for that ratio. Dotted line, ratio of 1 (equal size); values above 1 indicate the first-named group is larger. Ns, not significant. Abbreviations as in Figure 3.

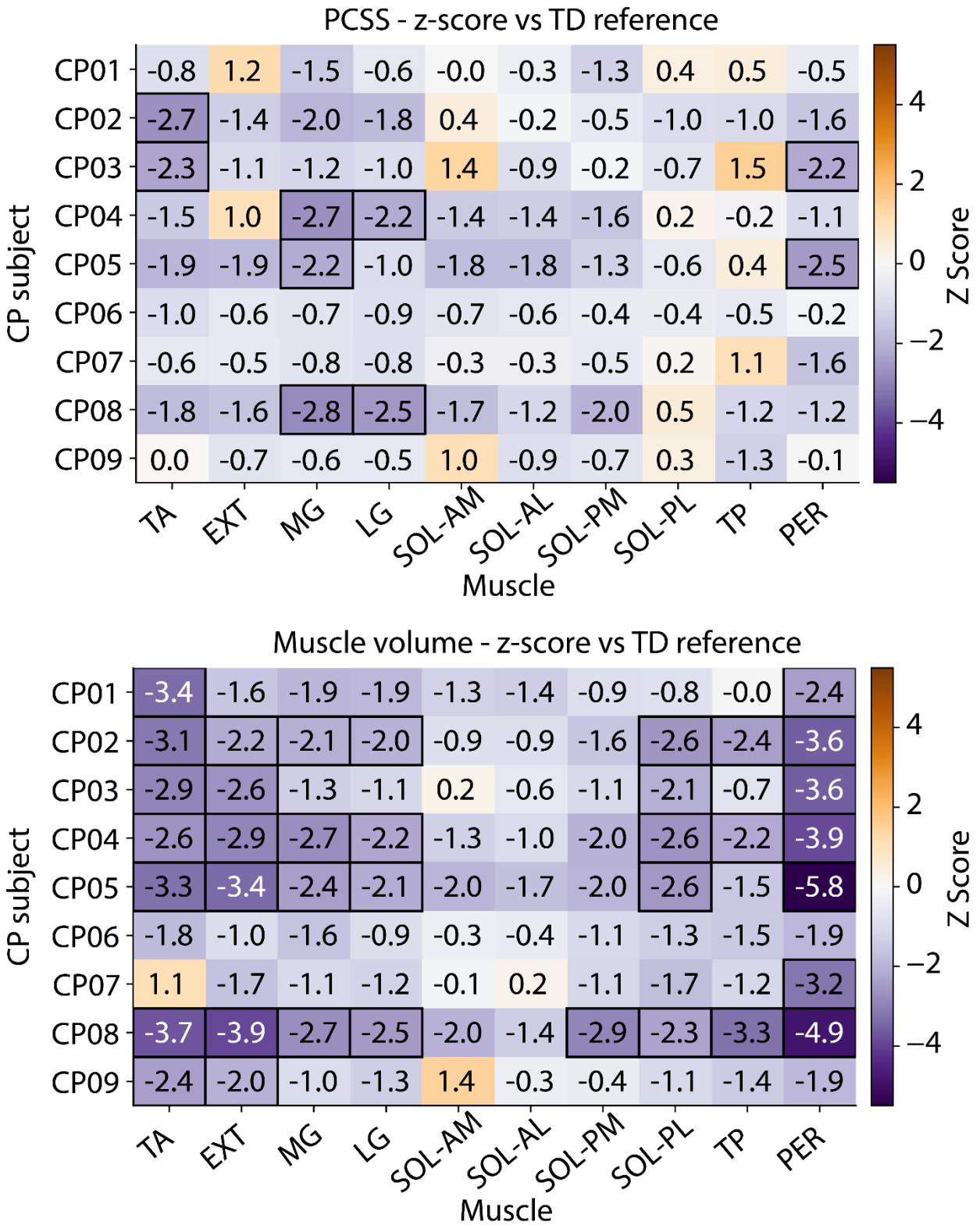


Figure 7. Individual CP z-scores for PCSS and muscle volume. Each cell is one CP participant's value for one region, expressed as a z-score against the TD mean and SD for that region and metric.

Negative (purple) indicates below the TD mean. Bold values with a black outline mark |z| > 2. Abbreviations as in Figure 1.

Composition of the volume deficit

Volume can fall because fascicles shorten, because the muscle thins across the fiber direction, or both, and the four functional groups differed in which of these applied. In the dorsiflexors, PCSS was reduced by 26.6% while fascicle length was unchanged (−0.9%, p_fdr = 0.89), so the loss was almost entirely cross-sectional. The invertor showed the reverse: fascicle length fell by 26.1% (p_fdr = 0.016) with cross-sectional tissue preserved (PCSS −3.4%, p_fdr = 0.86). The plantarflexors lost both dimensions in comparable proportion (PCSS −28.6%, fascicle length −31.5%), falling close to the line of proportional reduction, and the evertors were intermediate, weighted toward the cross-sectional axis (−36.0% and −16.1%). Individual muscles within each group followed the same arrangement (Fig. 8).

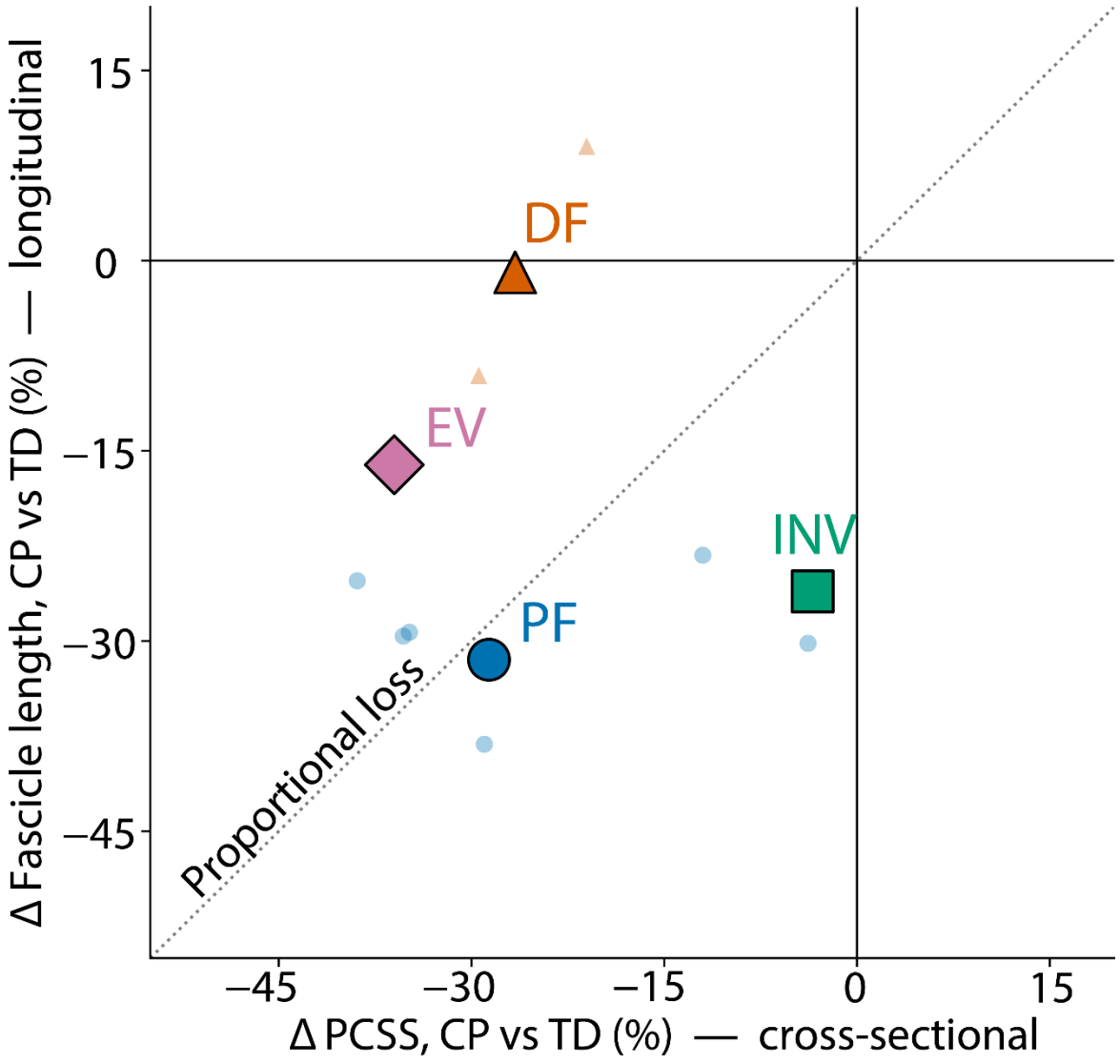


Figure 8. Decomposition of the volume deficit into cross-sectional and longitudinal components, by functional group. Percent change (CP vs. TD) in PCSS (x-axis) plotted against percent change in fascicle length (y-axis). Large markers show functional-group means; small, faded markers show individual muscles, colored by group. The dotted diagonal marks proportional loss. Abbreviations as in Figure 1&3.

Disproportionate regional deficits

Thirteen of 80 comparisons reached p_fdr < 0.05, all involving muscle length, fascicle length, fascicle angle, tortuosity or FA. No region differed for relative volume, PCSS or MD (Fig. 9).

In the dorsiflexors, differences were consistently positive. In EXT, fascicle length was relatively spared (+0.46, g = 1.68, p_fdr = 0.011), as were muscle length (+0.11, g = 1.47, p_fdr = 0.023) and FA (+0.12, g = 1.32, p_fdr = 0.019). FA was also relatively higher in TA (+0.17, g = 1.88, p_fdr = 0.003), whereas fascicle angle in TA was relatively lower (−0.22, g = −1.80, p_fdr = 0.019).

Among the plantarflexors, differences were mixed. Fascicle length was disproportionately reduced in SOL-PM (−0.21, g = −1.72, p_fdr = 0.011) and tortuosity relatively increased (+0.02, g = 1.40, p_fdr = 0.049), yet relative muscle length in the same region was higher than in TD (+0.11, g = 1.26, p_fdr = 0.023). FA was disproportionately reduced in SOL-AL (−0.14, g = −1.62, p_fdr < 0.001), SOL-AM (−0.13, g = −1.57, p_fdr = 0.009) and SOL-PL (−0.10, g = −1.55, p_fdr = 0.009). Relative muscle length was disproportionately reduced in MG (−0.09, g = −1.37, p_fdr = 0.023) and LG (−0.11, g = −1.38, p_fdr = 0.023).

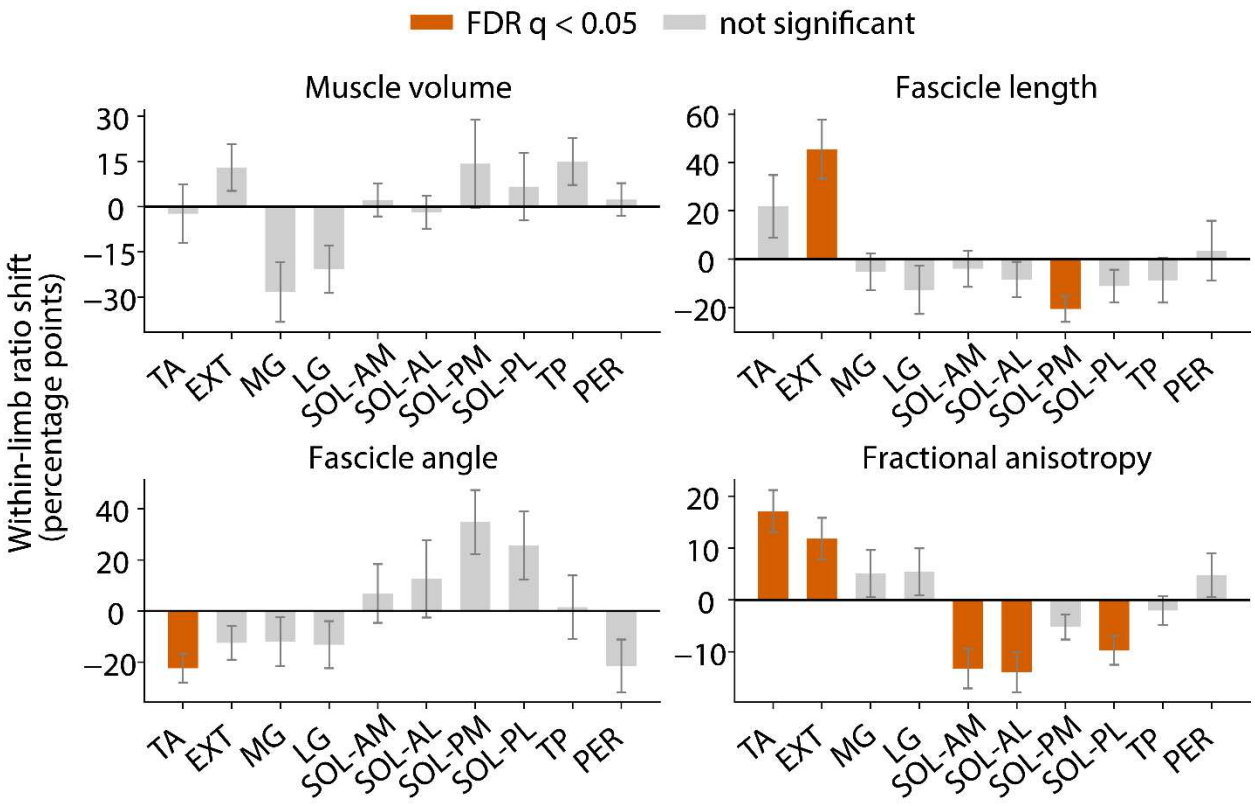


Figure 9. Within-limb distribution of deficits in CP. Each region is first expressed as a fraction of that participant's own limb average; bars show the group difference in that fraction (CP − TD) ± SEM of the difference. Zero indicates the region occupies the same position within the limb in both groups; above zero, relatively spared; below zero, disproportionately affected. These are not absolute group differences (see Figure 3). Orange, FDR q < 0.05 (exact permutation test, corrected across the ten regions within each metric); grey, not significant. Abbreviations as in Figure 1.

Robustness

All 13 regional findings remained significant on the unadjusted permutation test when any single participant was removed (largest leave-one-out p = 0.021). None of the four agonist–antagonist ratios reached significance in any leave-one-out iteration.

Discussion

Across the examined ankle muscles, the CP group showed consistently smaller and shorter morphology together with altered fascicle architecture. Volume was reduced to a similar extent in all four functional groups (−29% to −41%), and normalized muscle length was reduced in every group (−9.5% to −12.2%), indicating that the deficit was generalized rather than limited to a particular functional group. This aligns with previous studies reporting smaller muscle size in CP, which suggests both reduced force capacity and an altered operating range (2,28,29). Impaired neuromuscular drive, reduced loading, and constrained bone growth during development likely combine to limit longitudinal muscle growth and cross-sectional hypertrophy, reinforcing a smaller, shorter muscle–tendon unit (2,12,29). Functionally, a shorter normalized muscle and fascicle length is consistent with a shortened muscle–tendon unit, which can shift the muscle's operating point along the force–length curve, limiting active force production across the joint range where gait typically demands it for mid-stance dorsiflexion control and late-stance plantarflexion (27,30).

Although muscle was lost throughout the ankle, the balance between opposing muscle groups was preserved: neither the plantarflexor-to-dorsiflexor nor the invertor-to-evertor ratio of volume or PCSS differed between groups, and no comparison approached significance. This pattern is consistent with proportional muscle loss, although our sample size cannot establish equivalence. These data provide no support for attributing muscle remodeling in CP primarily to a plantarflexor-biased activation strategy (31), since chronic plantarflexor loading with dorsiflexor disuse would be expected to shift these ratios substantially. With the present sample, however, only a large shift would have been detectable, so the result argues against a large effect rather than against the

mechanism. Given the sample size, effects smaller than g = 1.41 could not be detected, so a modest imbalance cannot be excluded; the invertor-to-evertor PCSS ratio in particular differed in direction with a moderate effect size (g = 0.77) and warrants examination in a larger cohort.

Although the total amount of muscle deficit was proportional between antagonists, whether deficits were in muscle length or cross-section differed between muscle groups. That deficits differed between functional groups suggests that more than one growth process may be disturbed. A deficit confined to the cross-sectional axis, as in the dorsiflexors, is consistent with reduced radial hypertrophy under low mechanical demand while longitudinal growth remains intact, whereas a deficit confined to the longitudinal axis, as in the invertor, points instead to a failure to add length during growth. The plantarflexors, in which both dimensions fell together, are consistent with both processes operating. These are inferences from static architecture and cannot be confirmed in a cross-sectional design, but they indicate that describing all muscle change in CP as atrophy conflates mechanisms with different functional consequences, since cross-sectional loss lowers maximum force while fascicle shortening narrows the range over which force can be produced.

The dissociation between preserved dorsiflexor fascicle length and reduced plantarflexor and invertor fascicle length was clearer still when each region was expressed relative to the rest of that participant's own limb. In EXT, relative fascicle length, muscle length and FA were all higher in CP, as was relative FA in TA. The deep plantarflexors showed the opposite pattern: relative fascicle length was reduced in SOL-PM (−0.21, g = −1.72, q = 0.011), and relative FA was reduced in SOL-AM, SOL-AL and SOL-PL (all $q \leq 0.009$). These are within-limb comparisons and carry no implication that the dorsiflexors were spared in absolute terms, since dorsiflexor volume, muscle

length and PCSS were all reduced. What they identify is where the deficit is concentrated once its overall magnitude is accounted for, and that location is the deep soleus rather than the limb as a whole.

Fascicle orientation showed the same concentration of change in specific regions. Mean fascicle angle did not survive correction in any functional group, although the plantarflexor increase was close to threshold (+32.2%, $g = 1.28$, $q = 0.053$) and is more plausibly power-limited than absent. Pooling individual fascicles nonetheless revealed changes in the shape of the orientation distribution in two regions. In TA the upper tail was compressed; in SOL-PM the distribution widened across its whole range. The fascicle field therefore became more uniformly aligned in TA and more disordered in SOL-PM, two opposite forms of remodeling in muscles belonging to opposing functional groups. Mean and spread moved together here, but they carry different information: the mean locates the distribution, while the percentile and SD descriptors show that the change is confined to the upper tail in TA and spread across the whole distribution in SOL-PM.

Reported fascicle-length findings in CP are inconsistent, and the present result falls on one side of that divide. MG fascicle length here was 25.2% shorter than TD ($q = 0.019$), consistent with D'Souza et al., who found MG fascicles 4.2 mm shorter in children with CP and ankle contractures than in controls (19). Others have found no such difference: neither normalized SOL fascicle length (12) nor MG fascicle length at the neutral ankle position (32) differed between groups. Differences in normalization reference (height versus segment length), ankle position during scanning, cohort contracture status, and tractography parameters could each independently account for these

447 divergent results and cannot be distinguished with the present data. Resolving this will require a
448 study matching these factors directly.
449
450 In CP, dorsiflexor–plantarflexor coactivation has been proposed as a strategy to increase joint
451 stability during balance control (21), and co-contraction has been identified as a major contributor
452 to the elevated energy cost of walking in this population (33), although a more recent study in a
453 predominantly GMFCS level I cohort found no relation between a co-activation index and energy
454 cost (34). Because electromyography was not acquired in this study, coactivation could not be
455 measured, and this mechanism is considered here only as a candidate explanation for the
456 architectural pattern observed. With a smaller plantarflexor unit and reduced plantarflexor PCSS,
457 plantarflexor activation may contribute more to joint stiffness than to useful propulsion. Shorter
458 plantarflexor fascicles would further limit the excursion available for late-stance push-off. The
459 relative sparing of dorsiflexor fascicle length, alongside a smaller and shorter TA in absolute terms,
460 is compatible with continued dorsiflexor recruitment for foot clearance despite reduced overall
461 size, although this remains an inference in the absence of activation data.
462
463 One important note is that we did not directly measure sarcomere length, which determines where
464 fibers operate on the force–length relationship and therefore influences active force capacity
465 (27,30). Previous studies in CP have reported abnormally long resting sarcomere lengths and
466 reduced serial sarcomere number in ankle plantarflexor (35). Because fascicle length reflects the
467 product of serial sarcomere number and resting sarcomere length, our finding of shorter
468 normalized fascicle length cannot distinguish fewer sarcomeres in series from longer resting
469 sarcomere length, or a combination of both (2). The SOL-PM illustrates this ambiguity directly:

relative to the rest of the limb, its muscle belly length was preserved while its fascicle length was disproportionately reduced, consistent with a muscle–tendon unit that grew via tendon lengthening rather than proportional serial sarcomere addition (36).

Between-group differences in the soleus were not limited to global morphology but showed clear compartment-specific differences: on fascicle length, orientation and tortuosity SOL-PM was the most affected compartment, whereas on FA the deficit was concentrated in SOL-AM, SOL-AL and SOL-PL. SOL-AM was spared on every size and length measure yet showed one of the largest disproportionate FA deficits in the study, so no single compartment is uniformly most affected. Such compartment-specific patterns might be masked by whole-muscle measures, and are consistent with prior reports of heterogeneity in muscle size and architecture in CP (29,37,38). Statistical shape modelling offers a complementary approach to the compartment-wise analysis used here, representing spatial variation in morphology through a small number of modes rather than regional summaries. It has revealed localized shape differences in the SOL in spastic CP (39), and has recently been extended to incorporate DTI-derived fascicle orientation in the MG (40). Applying a similar tractography-derived SSM approach to SOL would be a next step to quantify region-specific architectural heterogeneity *in vivo* and correlating it with neuromuscular control and differential treatment responses in patients with CP.

Diffusion tensor differences were also regionally specific. FA did not differ at the level of functional groups, but was lower in the SOL-AL and SOL-PL soleus in absolute terms, and relative to the rest of the limb was lower across three soleus subregions and higher in both dorsiflexors. Reduced FA indicates lower directional coherence of diffusion, which may reflect disrupted

fascicle alignment or an altered extracellular environment (17), but it is not specific to architecture: intramuscular fat infiltration (41), common in more severely affected CP muscle, adds an isotropic component that lowers FA independently of fascicle organization. The present data cannot separate these mechanisms from true architectural remodeling. As above, this regional specificity in diffusion metrics parallels the architectural heterogeneity already noted in the soleus. MD was lower in TA (−7.4%) but did not differ in any other region, and showed no regional pattern once whole-limb differences were accounted for. One interpretation is that dorsiflexor tissue changes do not mirror plantarflexor changes and may follow a different remodeling pathway, although with a single significant region this remains tentative.

Clinically, these findings argue for matching interventions to the specific architectural deficit rather than treating the ankle muscles as a single unit. Cross-sectional and longitudinal deficits constrain function differently, so they are likely to respond to different stimuli. In the dorsiflexors, where the deficit was predominantly cross-sectional and fascicle length was relatively preserved, hypertrophy-oriented approaches such as progressive resistance training or neuromuscular electrical stimulation are the more direct target (42). In the invertor and plantarflexors, where fascicles were shorter, interventions that promote serial sarcomere addition, such as eccentric loading at long muscle lengths (43), may matter more than strengthening alone, although it remains uncertain whether CP muscle responds similarly to eccentric loading. Wearable technologies offer a further route to targeted loading: ankle exoskeletons that resist or assist specific phases of gait can concentrate training on the plantarflexors during push-off within a functional task (44). Finally, because the changes were regionally heterogeneous, imaging assessments of whole-muscle or 2D ultrasound representations of fascicles may not capture the most important features from which to

base rehabilitation. To this end, DTI-based compartment-resolved architecture could instead be used both to stratify participants and to quantify mechanism-specific responses for rehabilitation trials. Currently, most of our knowledge on CP muscle adaptations are inferred from cross-sectional studies in small cohorts; future work should increasingly explore prospective observations in intervention studies.

This study has several limitations. The sample of nine participants per group limits statistical power: only effects of g = 1.41 or larger could be detected with 80% power, so the non-significant findings reported here, including the preserved agonist–antagonist ratios, indicate that a difference could not be detected rather than that none exists. Despite DTI preprocessing, susceptibility- and motion-related distortions likely reduced diffusion signal quality and the reliability of tractography. Electromyography was not acquired, so coactivation was not measured and its relationship to the architectural differences observed here remains untested. Sarcomere length, strength and joint power were not measured. Future work should integrate these assessments in a larger cohort.

Conclusion

In children with CP, ankle muscles in all four functional groups were smaller and shorter than in TD controls, with volume deficits of 29–41%. Despite these deficits, we found no evidence of imbalance between antagonist groups: neither the plantarflexor-to-dorsiflexor nor the invertor-to-evertor ratio of muscle volume or PCSS differed from controls, although our sample size allows only large differences to be excluded. Whether CP muscles showed deficits in the longitudinal or cross-sectional axis depended on the muscle group. The deficit was almost entirely in cross-section in the dorsiflexors, almost entirely in length in the invertor, and both cross-section and length in

the plantarflexors. Architectural remodeling was also uneven within the limb. Relative to each participant's own limb average, the dorsiflexors showed no disproportionate architectural change, whereas fascicle length was selectively reduced in the SOL-PM, and FA was reduced in three of the four SOL compartments. Muscle loss in CP was therefore broadly proportional across antagonist groups, while the architecture was altered compartment by compartment. These findings suggest that interventions may be more effective when matched to the dimension and compartment affected rather than applied uniformly across the ankle: for example, hypertrophy-oriented training where cross-sectional area is lost, and length-oriented interventions where longitudinal growth is deficient. They also support compartment-resolved imaging as an outcome measure in rehabilitation trials.

Abbreviations

3D: Three-dimensional

AL: Anterolateral

AM: Anteromedial

CP: Cerebral palsy

DF: Dorsiflexor

DTI: Diffusion tensor imaging

EV: Evertor

EXT: Extensor group

FA: Fractional anisotropy

FDR: False discovery rate

GMFCS: Gross Motor Function Classification System

INV: Invertor

IQR: Interquartile range

LG: Lateral gastrocnemius

MD: Mean diffusivity

MG: Medial gastrocnemius

MRI: Magnetic resonance imaging

PCSS: Physiological cross-sectional surface(s) PMC

PER: Peroneals

PF: Plantarflexor

PL: Posterolateral

PM: Posteromedial

SD: Standard deviation

SEM: Standard error of the mean

SOL: Soleus

TA: Tibialis anterior

TD: Typically developing

TE: Echo time

TP: Tibialis posterior

TR: Repetition time

Declarations

Ethics approval and consent to participate

That study's protocol was approved by the University of Auckland Human Participants Ethics Committee. Written informed consent was obtained from the participants' parents or legal guardians before participation, and all children provided assent to take part in the study.

Consent for publication

Not applicable.

Availability of data and materials

The datasets generated and/or analyzed during this study are available from the corresponding author upon reasonable request.

Competing interests

The authors declare that they have no competing interests.

Funding

This study is funded by Department of Orthopaedics, University of North Carolina at Chapel Hill.

Authors' contributions

Z.L. undertook imaging processing, data analysis, figure generation, and main manuscript writing. G.H. conceptualized study, oversaw study execution, provided critical review of written manuscript.

Acknowledgement

We gratefully acknowledge the use of data originally collected with support from the Wishbone Trust, NZ Orthopaedic Association. We thank Maanya Bhutani, Adarsh Dandamudi, Chetan Daswani, and Kyle Royster for their assistance in segmentation. We also acknowledge the support of the UNC Department of Orthopaedics and the Lampe Joint Department of Biomedical Engineering for this project.

References

1. Oskoui M, Coutinho F, Dykeman J, Jetté N, Pringsheim T. An update on the prevalence of cerebral palsy: a systematic review and meta-analysis. Dev Med Child Neurol. 2013 Jun 1;55(6):509–19. doi:https://doi.org/10.1111/dmcn.12080

2. Handsfield GG, Williams S, Khuu S, Lichtwark G, Stott NS. Muscle architecture, growth, and biological Remodelling in cerebral palsy: a narrative review. BMC Musculoskeletal Disorders. BioMed Central Ltd; 2022. doi:10.1186/s12891-022-05110-5 PubMed PMID: 35272643.

3. Howard JJ, Graham K, Shortland AP. Understanding skeletal muscle in cerebral palsy: a path to personalized medicine? Developmental Medicine and Child Neurology. John Wiley and Sons Inc; 2022. p. 289–95. doi:10.1111/dmcn.15018 PubMed PMID: 34499350.

4. Williams SA, Stott NS, Valentine J, Elliott C, Reid SL. Measuring skeletal muscle morphology and architecture with imaging modalities in children with cerebral palsy: a scoping review. Dev Med Child Neurol. 2021 Mar 1;63(3):263–73. doi:https://doi.org/10.1111/dmcn.14714

5. Fregly BJ, Boninger ML, Reinkensmeyer DJ. Personalized neuromusculoskeletal modeling to improve treatment of mobility impairments: a perspective from European research sites. J Neuroeng Rehabil. 2012;9(1):18. doi:10.1186/1743-0003-9-18

6. Ippersiel P, Dussault-Picard C, Mohammadyari SG, De Carvalho GB, Chandran VD, Pal S, et al. Muscle coactivation during gait in children with and without cerebral palsy. Gait Posture. 2024 Feb 1;108:110–6. doi:10.1016/j.gaitpost.2023.11.012 PubMed PMID: 38029482.

7. Ateş F, Temelli Y, Yucesoy CA. Effects of antagonistic and synergistic muscles' co-activation on mechanics of activated spastic semitendinosus in children with cerebral palsy. Hum Mov Sci. 2018 Feb 1;57:103–10. doi:10.1016/j.humov.2017.11.011 PubMed PMID: 29197788.

8. Gross R, Leboeuf F, Hardouin JB, Perrouin-Verbe B, Brochard S, Rémy-Néris O. Does muscle coactivation influence joint excursions during gait in children with and without hemiplegic cerebral palsy? Relationship between muscle coactivation and joint kinematics. Clinical Biomechanics. 2015 Dec 1;30(10):1088–93. doi:10.1016/j.clinbiomech.2015.09.001 PubMed PMID: 26377949.

9. Davis JF, Khir AW, Barber L, Reeves ND, Khan T, DeLuca M, et al. The mechanisms of adaptation for muscle fascicle length changes with exercise: Implications for spastic muscle. Med Hypotheses. 2020 Nov 1;144. doi:10.1016/j.mehy.2020.110199 PubMed PMID: 33254508.

10. Mathewson MA, Chambers HG, Girard PJ, Tenenhaus M, Schwartz AK, Lieber RL. Stiff muscle fibers in calf muscles of patients with cerebral palsy lead to high passive muscle stiffness. Journal of Orthopaedic Research. 2014 Dec 1;32(12):1667–74. doi:10.1002/jor.22719 PubMed PMID: 25138654.

11. Åhblom A, Pontén E, Destro A, Petersson S, von Walden F, Wang R, et al. Exploration of the triceps surae muscle in ambulatory children with cerebral palsy using instrumented measurements of stiffness and diffusion tensor magnetic resonance imaging for muscle architecture. BMC Musculoskelet Disord. 2024 Dec 1;25(1). doi:10.1186/s12891-024-07890-4 PubMed PMID: 39394126.

12. Sahrmann AS, Stott NS, Besier TF, Fernandez JW, Handsfield GG. Soleus muscle weakness in cerebral palsy: Muscle architecture revealed with Diffusion Tensor Imaging. PLoS One. 2019 Feb 1;14(2). doi:10.1371/journal.pone.0205944 PubMed PMID: 30802250.

13. Varghese RA, Rebello G, Shah H, Joseph B. Biomechanical Basis for Treatment of Pediatric Foot Deformities Part II: Pathomechanics of Common Foot Deformities. Journal of the Pediatric Orthopaedic Society of North America. 2022;4(2):464. doi:https://doi.org/10.55275/JPOSNA-2022-0038

14. Hof AL, Duysens J. Responses of human ankle muscles to mediolateral balance perturbations during walking. Hum Mov Sci. 2018 Feb 1;57:69–82. doi:10.1016/j.humov.2017.11.009 PubMed PMID: 29174418.

15. Dick TJM, Hug F. Advances in imaging for assessing the design and mechanics of skeletal muscle in vivo. Journal of Biomechanics. Elsevier Ltd; 2023. doi:10.1016/j.jbiomech.2023.111640 PubMed PMID: 37244210.

16. Bolsterlee B, D'Souza A, Herbert RD. Reliability and robustness of muscle architecture measurements obtained using diffusion tensor imaging with anatomically constrained tractography. J Biomech. 2019 Mar 27;86:71–8. doi:10.1016/j.jbiomech.2019.01.043 PubMed PMID: 30739766.

17. Martín-Noguerol T, Barousse R, Wessell DE, Rossi I, Luna A. Clinical applications of skeletal muscle diffusion tensor imaging. Skeletal Radiology. Springer Science and Business Media Deutschland GmbH; 2023. p. 1639–49. doi:10.1007/s00256-023-04350-3 PubMed PMID: 37083977.

18. Berry DB, Gordon III JA, Adair V, Frank LR, Ward SR. From Voxels to Physiology: A Review of Diffusion Magnetic Resonance Imaging Applications in Skeletal Muscle. Journal of Magnetic Resonance Imaging. 2025 Feb 1;61(2):595–615. doi:https://doi.org/10.1002/jmri.29489

19. D'Souza A, Bolsterlee B, Lancaster A, Herbert RD. Muscle architecture in children with cerebral palsy and ankle contractures: an investigation using diffusion tensor imaging. Clinical Biomechanics. 2019 Aug 1;68:205–11. doi:10.1016/j.clinbiomech.2019.06.013 PubMed PMID: 31255994.

20. Bolsterlee B, Chow BVY, Davies S, Morgan C, Rae CD, Warton DI, et al. Triceps surae muscle architecture in ambulant children with cerebral palsy: architectural adaptations vary between children and muscles. J Biomech. 2026;202:113286. doi:https://doi.org/10.1016/j.jbiomech.2026.113286

21. Willaert J, Ting LH, Van Campenhout A, Desloovere K, De Groote F. Increased coactivation during clinical tests of spasticity is associated with increased coactivation during reactive standing balance control in cerebral palsy. J Neurophysiol. 2025 Jul 1;134(1):118–27. doi:10.1152/jn.00568.2024 PubMed PMID: 40499562.

22. Bolsterlee B, Finni T, D'Souza A, Eguchi J, Clarke EC, Herbert RD. Three-dimensional architecture of the whole human soleus muscle in vivo. PeerJ. 2018;2018(4). doi:10.7717/peerj.4610

23. Isensee F, Rokuss M, Krämer L, Dinkelacker S, Ravindran A, Stritzke F, et al. nnInteractive: Redefining 3D Promptable Segmentation [Internet]. 2025 Mar 11. Available from: http://arxiv.org/abs/2503.08373

24. Yushkevich PA, Piven J, Hazlett HC, Smith RG, Ho S, Gee JC, et al. User-guided 3D active contour segmentation of anatomical structures: Significantly improved efficiency and reliability. Neuroimage. 2006 Jul 1;31(3):1116–28. doi:10.1016/j.neuroimage.2006.01.015 PubMed PMID: 16545965.

25. Tournier JD, Smith R, Raffelt D, Tabbara R, Dhollander T, Pietsch M, et al. MRtrix3: A fast, flexible and open software framework for medical image processing and

visualisation. NeuroImage. Academic Press Inc.; 2019. doi:10.1016/j.neuroimage.2019.116137 PubMed PMID: 31473352.

26. Liu Z, Duncombe P, Napadow V, Handsfield G. Physiological Cross-Sectional Surfaces: A Method for Estimating Muscle Functional Capacity from 3D Digital Models of Fiber Architecture. bioRxiv. 2026 Jan 1;2026.07.20.739018. doi:10.64898/2026.07.20.739018

27. Lieber RL, Ward SR. Skeletal muscle design to meet functional demands. Philosophical Transactions of the Royal Society B: Biological Sciences. 2011;366(1570):1466–76. doi:10.1098/rstb.2010.0316 PubMed PMID: 21502118.

28. Barrett RS, Lichtwark GA. Gross muscle morphology and structure in spastic cerebral palsy: a systematic review. Developmental Medicine and Child Neurology. Blackwell Publishing Ltd; 2010. p. 794–804. doi:10.1111/j.1469-8749.2010.03686.x PubMed PMID: 20477832.

29. Handsfield GG, Meyer CH, Abel MF, Blemker SS. Heterogeneity of muscle sizes in the lower limbs of children with cerebral palsy. Muscle Nerve. 2016 Jun 1;53(6):933–45. doi:10.1002/mus.24972 PubMed PMID: 26565390.

30. Lieber RL, Theologis T. Muscle-tendon unit in children with cerebral palsy. Dev Med Child Neurol. 2021;63(8):908–13. doi:10.1111/dmcn.15458

31. Gracies JM. Pathophysiology of spastic paresis. II: Emergence of muscle overactivity. Muscle Nerve. 2005 May 1;31(5):552–71. doi:https://doi.org/10.1002/mus.20285

32. BARBER LEE, HASTINGS-ISON T, BAKER R, BARRETT ROD, LICHTWARK G. Medial gastrocnemius muscle volume and fascicle length in children aged 2 to 5 years with cerebral palsy. Dev Med Child Neurol. 2011 Jun 1;53(6):543–8. doi:https://doi.org/10.1111/j.1469-8749.2011.03913.x

33. UNNITHAN V, DOWLING J, FROST G, BAR-OR O. Role of cocontraction in the O2 cost of walking in children with cerebral palsy. Med Sci Sports Exerc. 1996;28(12):1498–504.

34. Gagnat Y, Brændvik SM, Ringheim I, Roeleveld K. The relation of energy cost of walking with gait deviation, asymmetry, and lower limb muscle co-activation in children with cerebral palsy: a retrospective cross-sectional study. BMC Musculoskelet Disord. 2023;24(1):111. doi:10.1186/s12891-023-06223-1

35. Mathewson MA, Ward SR, Chambers HG, Lieber RL. High resolution muscle measurements provide insights into equinus contractures in patients with cerebral palsy. Journal of Orthopaedic Research. 2015 Jan 1;33(1):33–9. doi:10.1002/jor.22728 PubMed PMID: 25242618.

36. Wren T, Cheatwood A, Rethlefsen S, Hara R, Perez F, Kay R. Achilles Tendon Length and Medial Gastrocnemius Architecture in Children With Cerebral Palsy and Equinus Gait. Journal of Pediatric Orthopaedics. 2010;30(5):479–84. doi:10.1097/BPO.0b013e3181e00c80

37. Hanssen B, Peeters N, Vandekerckhove I, De Beukelaer N, Bar-On L, Molenaers G, et al. The Contribution of Decreased Muscle Size to Muscle Weakness in Children With Spastic Cerebral Palsy. Front Neurol. 2021 Jul 26;12. doi:10.3389/fneur.2021.692582

38. Bolsterlee B, Chow BVY, Yu J, Davies S, Morgan C, Rae CD, et al. Childhood muscle growth: Reference curves for lower leg muscle volumes and their clinical application in cerebral palsy. Proc Natl Acad Sci U S A. 2025 Apr 8;122(14). doi:10.1073/pnas.2416660122 PubMed PMID: 40163724.

39. Bin Ghouth SG, Williams SA, Reid SL, Besier TF, Handsfield GG. A statistical shape model of soleus muscle morphology in spastic cerebral palsy. Sci Rep. 2022 Dec 1;12(1). doi:10.1038/s41598-022-11611-z PubMed PMID: 35546597.

40. Bin Ghouth S, Besier T, Handsfield G. Statistical Shape and Fibre Orientation Model for Muscle Architecture Characterisation of the Medial Gastrocnemius. Ann Biomed Eng. 2025;53(12):3376–88. doi:10.1007/s10439-025-03866-0

41. Noble JJ, Charles-Edwards GD, Keevil SF, Lewis AP, Gough M, Shortland AP. Intramuscular fat in ambulant young adults with bilateral spastic cerebral palsy. BMC Musculoskelet Disord. 2014 Jul 12;15(1). doi:10.1186/1471-2474-15-236 PubMed PMID: 25016395.

42. Pool D, Elliott C, Bear N, Donnelly CJ, Davis C, Stannage K, et al. Neuromuscular electrical stimulation-assisted gait increases muscle strength and volume in children with unilateral spastic cerebral palsy. Dev Med Child Neurol. 2016 May 1;58(5):492–501. doi:10.1111/dmcn.12955 PubMed PMID: 26555148.

43. Pincheira PA, Boswell MA, Franchi M V, Delp SL, Lichtwark GA. Biceps femoris long head sarcomere and fascicle length adaptations after 3 weeks of eccentric exercise training. J Sport Health Sci. 2022;11(1):43–9. doi:https://doi.org/10.1016/j.jshs.2021.09.002

44. Conner BC, Remec NM, Orum EK, Frank EM, Lerner ZF. Wearable Adaptive Resistance Training Improves Ankle Strength, Walking Efficiency and Mobility in Cerebral Palsy: A Pilot Clinical Trial. IEEE Open J Eng Med Biol. 2020;1:282–9. doi:10.1109/OJEMB.2020.3035316